Fast evolution of SARS-CoV-2 BA.2.86 to JN.1 under heavy immune pressure

Sijie Yang[1,2,3,#], Yuanling Yu[2,#], Yanli Xu[4], Fanchong Jian[1,2,5], Weiliang Song[1,2,6], Ayijiang Yisimayi[1,2,6], Peng Wang[2], Jing Wang[2], Jingyi Liu[1,2,7], Lingling Yu[2], Xiao Niu[1,2,6], Jing Wang[1,2,6], Yao Wang[2], Fei Shao[2], Ronghua Jin[4], Youchun Wang[2,8], Yunlong Cao[1,2,6,*]

[1]Biomedical Pioneering Innovation Center (BIOPIC), Peking University, Beijing, P. R. China.

[2]Changping Laboratory, Beijing, P. R. China.

[3]Peking-Tsinghua Center for Life Sciences, Tsinghua University, Beijing, P. R. China.

[4]Beijing Ditan Hospital, Capital Medical University, Beijing, P. R. China.

[5]College of Chemistry and Molecular Engineering, Peking University, Beijing, P. R. China.

[6]School of Life Sciences, Peking University, Beijing, P. R. China.

[7]College of Future Technology, Peking University, Beijing, P. R. China.

[8]Institute of Medical Biology, Chinese Academy of Medical Science & Peking Union Medical College, Kunming, P. R. China

[*]Correspondence: Yunlong Cao (yunlongcao@pku.edu.cn).

[#]These authors contributed equally.

Abstract

While the BA.2.86 variant demonstrated significant antigenic drift and enhanced ACE2 binding affinity, its ability to evade humoral immunity was relatively moderate compared to dominant strains like EG.5 and HK.3. However, the emergence of a new subvariant, JN.1 (BA.2.86.1.1), which possesses an additional spike mutation, L455S, compared to BA.2.86, showed a markedly increased prevalence in Europe and North America, especially in France. Here, we found that L455S of JN.1 significantly enhances immune evasion capabilities at the expense of reduced ACE2 binding affinity. This mutation enables JN.1 to effectively evade Class 1 neutralizing antibodies, offsetting BA.2.86's susceptibility and thus allowing it to outcompete both its precursor BA.2.86 and the prevailing variants HV.1 (XBB.1.5+L452R+F456L) and JD.1.1 (XBB.1.5+L455F+F456L+A475V) in terms of humoral immune evasion. The rapid evolution from BA.2.86 to JN.1, similar to the earlier transition from BA.2.75 to CH.1.1, highlights the importance of closely monitoring strains with high ACE2 binding affinity and distinct antigenicity, despite their unremarkable immune evasion capabilities. Such strains have the potential to quickly accumulate mutations that enhance their immune escape during transmission, often at the cost of receptor binding.

35 The saltation variant BA.2.86, which was quickly designated as a variant under monitoring (VUM) after its emergence, has garnered global attention. Although BA.2.86 did not exhibit significant immune escape compared to dominant variants, it demonstrated remarkable ACE2 binding affinity[1-5]. This increased binding affinity, coupled with its distinct antigenicity, enabled BA.2.86 to accumulate mutations during transmission, potentially enhancing immune evasion while 40 possibly compromising receptor binding, akin to the previous evolution from BA.2.75 to CH.1.1[6-9]. Notably, with just one additional receptor binding domain (RBD) mutation, L455S, compared to its predecessor BA.2.86, the JN.1 variant rapidly became predominant in France (Figure A and Figure S1), surpassing both BA.2.86 and the "FLip" (L455F+F456L) strains, currently its most significant competitors. Consequently, a thorough investigation into the immune evasion 45 capability and mechanism of JN.1, particularly given its few additional mutations, is imperative.

We first study the humoral immune evasion of JN.1 and other circulating strains using pseudovirus-based neutralization assays with plasma from convalescent individuals from XBB infection. These individuals, having received three doses of inactivated vaccines, subsequently experienced XBB (XBB subvariants with S486P substitution) breakthrough infections (BTIs). Our 50 study included two cohorts, one with 27 participants who had post-vaccination XBB BTI and another with patients reinfected with XBB after BA.5 or BF.7 BTI. JN.1 displayed significantly enhanced immune escape compared to the ancestral variant BA.2.86. This was evidenced by a 2.1-fold decrease in 50% neutralization titers (NT50) among XBB reinfected individuals post-BA.5/BF.7 infection and a 1.1-fold decrease in NT50 in the XBB BTI convalescents (Figure 55 B and Figure S2). Additionally, JN.1's plasma evasion surpassed that of competitive variants HV.1 (EG.5+L452R) and JD.1.1 (FLip+A475V). Notably, these strains exhibited significantly lower plasma neutralization titers after acquiring L452R and A475V mutations, respectively, and were comparable to BA.2.86. This suggests that the antigenically distinct JN.1 strain significantly increased its immune evasion after acquiring the spike mutation L455S in its short-term evolution.

60 Subsequently, we measured the binding affinity between human ACE2 (hACE2) and the RBD of various Omicron subvariants using surface plasmon resonance (SPR). A notable reduction in ACE2 binding affinity was observed in JN.1, indicating that its enhanced immune escape capabilities come at the expense of reduced ACE2 binding (Figure C). A475V mutation in JD.1.1

(XBB.1.5 + FLip + A475V) also resulted in decreased binding affinity, enhancing immune evasion compared to HK.3 (XBB.1.5 + FLip). However, the L452R mutation did not significantly affect binding affinity. These findings prompt further investigation into how specific mutations influence immune evasion patterns, leading to a trade-off between ACE2 affinity and viral growth advantage.

Considering that the L455 is predominantly targeted RBD Class 1 antibodies, as indicated by prior research, our study further examined the evasion capabilities of JN.1 in response to eight XBB.1.5-neutralizing Class 1 monoclonal antibodies (mAbs) [7]. Pseudovirus neutralization assays demonstrated that the addition of the L455S mutation notably enhanced JN.1's ability to evade Class 1 antibodies. This mutation effectively compensated for BA.2.86's susceptibility to this antibody group, resulting in a 46-fold increase in 50% inhibitory concentration (IC50) values (Figure D). Similarly, the FLip + A475V variant (JD.1.1) exhibited increased resistance to Class 1 antibodies compared to the FLip variant (HK.3). However, JN.1's superior evasion of both class 2/3 and SD1-targeting antibodies enabled it to outperform JD.1.1 overall. In terms of therapeutic antibodies, SA55 retained its neutralizing efficacy against all examined variants (Figure E). Omi-42 remained effective against JN.1, although HK.3 showed slight evasion and JD.1.1 demonstrated significant evasion. These findings suggest that L455S enhances JN.1's resistance to humoral immunity, particularly mediated by the evasion of class 1 antibodies, relative to BA.2.86. Furthermore, these results offer insights into the recent trend of convergent A475V mutations among FLip variants, indicating substantially high immune pressure posed by Class 1 public neutralizing antibodies. The emergence of A475V in JD.1.1 and L455S in JN.1 may represent two distinct evolutionary paths converging toward evasion of such antibodies.

To sum up, JN.1, at the expense of reduced hACE2 binding, demonstrated enhanced immune evasion compared to BA.2.86 and other resistant strains like HV.1 and JD.1.1. Specifically, JN.1's spike mutation L455S effectively escapes Class 1 neutralizing antibodies. For BA.2.86, E554K specifically evades SD1-targeting antibodies, A484K and V483del enabled evasion of class 2 antibodies, and K356T, L452W, and P445H facilitated evasion of class 3 antibodies[1]. JN.1, by inheriting BA.2.86's antigenic diversity and adding L455S, achieves extensive resistance across RBD Class1/2/3 and SD1 antibodies. Additionally, BA.2.86’s high ACE2 binding affinity enables

the emergence and prevalence of evasive mutations like L445S that weaken hACE2-RBD interaction, maintaining the ACE2 binding affinity above a critical threshold for efficient cell entry. This evolutionary pattern, similar to the previous transition from BA.2.75 to CH.1.1[2,3,9], illustrates a shift from high ACE2 binding to increased evasion capacity, leading to successful prevalence. Overall, these findings underscore the complex interplay between ACE2 affinity and immune evasion. The potential of variants with high ACE2 binding affinity and distinct antigenicity to refine their evasion mechanisms by sacrificing ACE2 affinity warrants attention. Therefore, vigilant monitoring of BA.2.86 and JN.1 is essential, given the possibility of accumulating additional evasive mutations like FLip or A475V.

Acknowledgments

We are grateful to scientists in the community for their continuous tracking of SARS-CoV-2 variants and helpful discussion. We thank all volunteers for providing blood samples. This project is financially supported by the Ministry of Science and Technology of China (2023YFC3041500; 2023YFC3043200), Changping Laboratory (2021A0201; 2021D0102), Peking University (2401113277; 8204800750), and the National Natural Science Foundation of China (32222030).

Author Contributions

Y.C. designed and supervised the study. S.Y. and Y.C. wrote the manuscript with inputs from all authors. Y.X. and R.J. recruited the SARS-CoV-2 convalescents. S.Y., F.J., W.S. and J.L performed sequence analysis and illustration. Y.Y. and Youchun W. constructed pseudoviruses. P.W., L.Y., Yao W., J.W. (BIOPIC), J.W. (Changping Laboratory) and F.S. processed the plasma samples and performed the pseudovirus neutralization assays. F.J., W.S., A.Y., X.N., and Y.C. analyzed the neutralization data.

Declaration of interests

Y.C. is the inventor of the provisional patent applications for BD series antibodies, which includes BD55-5514 (SA55). Y.C. is the founder of Singlomics Biopharmaceuticals. Other authors declare no competing interests.

120 **References**

1. Yang, S. et al. Antigenicity and infectivity characterisation of SARS-CoV-2 BA.2.86. The Lancet Infectious Diseases 23, e457–e459 (2023).

2. Wannigama, D. L. et al. Tracing the new SARS-CoV-2 variant BA.2.86 in the community through wastewater surveillance in Bangkok, Thailand. The Lancet Infectious Diseases 23,
125 e464–e466 (2023).

3. Wang, Q. et al. Antigenicity and receptor affinity of SARS-CoV-2 BA.2.86 spike. Nature 1–3 (2023) doi:10.1038/s41586-023-06750-w.

4. Uriu, K. et al. Transmissibility, infectivity, and immune evasion of the SARS-CoV-2 BA.2.86 variant. The Lancet Infectious Diseases 23, e460–e461 (2023).

130 5. Sheward, D. J. et al. Sensitivity of the SARS-CoV-2 BA.2.86 variant to prevailing neutralising antibody responses. The Lancet Infectious Diseases 23, e462–e463 (2023).

6. Cao, Y. et al. Characterization of the enhanced infectivity and antibody evasion of Omicron BA.2.75. Cell Host & Microbe 30, 1527-1539.e5 (2022).

7. Cao, Y. et al. Imprinted SARS-CoV-2 humoral immunity induces convergent Omicron RBD
135 evolution. Nature 614, 521–529 (2023).

8. Wang, X. et al. Neutralization of SARS-CoV-2 BQ.1.1, CH.1.1, and XBB.1.5 by breakthrough infection sera from previous and recent waves in China. Cell Discov 9, 1–4 (2023).

9. Wang, Q. et al. Evolving antibody evasion and receptor affinity of the Omicron BA.2.75 sublineage of SARS-CoV-2. iScience 26, 108254 (2023).

140 10. Jian, F. et al. Convergent evolution of SARS-CoV-2 XBB lineages on receptor-binding domain 455-456 enhances antibody evasion and ACE2 binding. 2023.08.30.555211 Preprint at https://doi.org/10.1101/2023.08.30.555211 (2023).

Methods Details

Patient recruitment and plasma isolation

145 As previously described, blood samples from convalescent patients who had recovered from SARS-CoV-2 Omicron BTI or reinfection were obtained following approved study protocols (Ethics Committee archiving No. LL-2021-024-02 and No. 2022N045KY)[1,2]. Patients in the reinfection cohorts experienced first infections in December 2022 in Beijing and Tianjin and the second infection between May and June 2023[3]. The time of infections for individuals in the XBB
150 BTI were between May and June 2023. The infections were confirmed by PCR test or antigen test while the viral strains of them were determined by sequencing.

After collection, whole blood samples were diluted 1:1 with PBS+2% FBS and then gradiently centrifugated with Ficoll (Cytiva, 17-1440-03). These plasma samples were then collected, aliquoted, stored at temperatures of -20 ° C or lower, and subjected to heat inactivation before
155 other experimental procedures.

Pseudovirus neutralization assay

Based on the vesicular stomatitis virus (VSV) pseudovirus packaging system, pseudovirus of SARS-CoV-2 variant spike was generated[4]. G* Δ G-VSV virus (VSV G pseudotyped virus, Kerafast) was added to the cell culture supernatant., The the pcDNA3.1 vector incorporating spike
160 gene which was optimized using a mammalian codon was transfected into 293T cells (American Type Culture Collection [ATCC], CRL-3216). After culture, the pseudovirus in the supernatant was harvested, filtered, aliquoted, and frozen at −80° C for subsequent use. Plasma samples or antibodies were serially diluted in culture media, then were with pseudovirus followed by a 1-hour incubation at 37 ° C in a 5% CO_2 incubator. Digested Huh-7 cells (Japanese Collection of
165 Research Bioresources [JCRB], 0403) were introduced into the antibody-virus mixture. After a day of incubation, the supernatant was removed. D-luciferin reagent (PerkinElmer, 6066769) was applied, left to incubate in darkness for 2 minutes. Then cells were lysed and transferred to the detection plates. A microplate spectrophotometer (PerkinElmer, HH3400) was used to detect the luminescence value and a four-parameter logistic regression model was employed to determine the
170 IC50 values.

Antigenic cartography construction

The serum obtained from mice that received two doses (10 μg) of spike mRNA from the WT, BA.5, BQ.1.1, or XBB strains was collected one week after the final immunization. Then the

pseudovirus assays were to conducted to generate the neutralization titer data. The preprocessed and normalized data were transformed using multidimensional scaling (MDS) to arrange the antigen and plasma points within the antigenic cartography. Following that, antigenic cartography was computed by the R package Racmacs (v1.1.35), and visualized by the R package ggplot2 (v3.4.1)[5].

Surface Plasmon Resonance

SPR measurements were performed on the constructed RBD of BA.2.86, JN.1 and XBB subvariants including HK.3,HV.1, EG.5 and JD.1.1 based on Biacore 8K (Cytiva). Human ACE2 tagged with Fc tag was immobilized onto Protein A sensor chips (Cytiva). After serial dilution (6.25, 12.5, 25, 50, and 100 nM), the purified RBD samples of SARS-CoV-2 variants were injected on sensor chips. Responses were captured by Biacore 8K Evaluation Software 3.0 (Cytiva) at room temperature, and the raw data were fitted to 1:1 binding model using Biacore 8K Evaluation Software 3.0 (Cytiva). Each strain underwent two or three independent replicates for validation.

Methods References

1. Yang, S. et al. Antigenicity and infectivity characterisation of SARS-CoV-2 BA.2.86. The Lancet Infectious Diseases 23, e457–e459 (2023).

2. Jian, F. et al. Convergent evolution of SARS-CoV-2 XBB lineages on receptor-binding domain 455-456 enhances antibody evasion and ACE2 binding. 2023.08.30.555211 Preprint at https://doi.org/10.1101/2023.08.30.555211 (2023).

3. Pan, Y., Wang, L., Feng, Z., Xu, H., Li, F., Shen, Y., Zhang, D., Liu, W.J., Gao, G.F., and Wang, Q. (2023). Characterisation of SARS-CoV-2 variants in Beijing during 2022: an epidemiological and phylogenetic analysis. The Lancet 401, 664-672. 10.1016/S0140-6736(23)00129-0.

4. Li, Q., Wu, J., Nie, J., Zhang, L., Hao, H., Liu, S., Zhao, C., Zhang, Q., Liu, H., Nie, L., et al. (2020). The Impact of Mutations in SARS-CoV-2 Spike on Viral Infectivity and Antigenicity. Cell 182, 1284-1294.e1289. 10.1016/j.cell.2020.07.012.

5. Smith, D.J., Lapedes, A.S., de Jong, J.C., Bestebroer, T.M., Rimmelzwaan, G.F., Osterhaus, A.D.M.E., and Fouchier, R.A.M. (2004). Mapping the Antigenic and Genetic Evolution of Influenza Virus. Science 305, 371-376. doi:10.1126/science.109721

204 **Figure Legends**

205 **Figure | JN.1 exhibits profound immune evasion and decreased ACE2 binding affinity**

206 (A) Sequence percentages of prevalent variants since August 2023 including JN.1, BA.2.86 (the
207 original BA.2.86 and its subvariants except JN.1), HV.1, FLip + A475V and HK.3. The growth
208 advantages relative to HK.3 in past 2 month of these strains are denoted in the legend within
209 parentheses. Data are collected from covSPECTRUM.

210 (B) The 50% neutralizing titer (NT50) of convalescent plasma against SARS-CoV-2 variants
211 measured in individuals who received three CoronaVac doses and had breakthrough infection with
212 BA.5 or BF.7 followed by XBB reinfection (n = 54). Labels for geometric mean titers (GMT) are
213 located above each group, with the fold changes and statistical significances indicated above the
214 GMT labels. Below the dashed line are labels specifying the numbers of negative samples which
215 are related to the limit of detection (NT50=20). Two-tailed Wilcoxon signed-rank tests of paired
216 samples were used. *p<0.05, **p<0.01, ***p<0.001, and ****p<0.0001.

217 (C) The human ACE2 (angiotensin-converting enzyme 2) binding affinities of HK.3
218 (XBB.1.5+L455F+F456L), BA.2.86, HV.1 (XBB.1.5+L452R+F456L), EG.5 (XBB.1.5+F456L),
219 JD.1.1 (XBB.1.5+L455F+F456L+A475V), and JN.1 (BA.2.86+L455S) RBD determined by SPR
220 sensorgrams. KD values (nM) are displayed above the bars, and all replicates are represented as
221 points.

222 (D) Class 1 neutralizing antibodies (NAbs) resistance against pseudovirus of XBB.1.5, EG.5,
223 HV.1, HK.3, JD.1.1, BA.2.86, and JN.1 strains indicated by the IC50 values (n=8). The values and
224 related fold changes when compared to D614G or other strains are labelled.

225 (E) The IC50 (ug/mL) of approved or candidate monoclonal neutralising antibody drugs targeting
226 spike are assessed against XBB.1.5, EG.5, HV.1, HK.3, JD.1.1, BA.2.86, and JN.1 pseudovirus.

227

228 **Supplementary Tables and Figures**

229 **Figure S1 | Sequence mutations of prevailing variants**

230 Mutations of XBB.1.5, HV.1, HK.3, JD.1.1, BA.2.86 and JN.1 on the spike glycoprotein. The
231 existence of mutations for each variant are indicated in purple. The sky-blue color denotes
232 relatively absent mutations. The spike locations of listed mutations are labeled on the right.

233 **Figure S2 | Neutralization of BA.2.86 against plasma from XBB BTI patients**

234 Related to Figure B. NT50 against SARS-CoV-2 variants of convalescent plasma who received
235 three CoronaVac doses and experienced XBB breakthrough infection (n = 27). The GMT values
236 together with the relative fold changes and statistical significances are labelled above each group,
237 and labels for the numbers of negative samples are below the dashed line which are related to the
238 limit of detection (NT50=20). Two-tailed Wilcoxon signed-rank tests of paired samples were used.
239 *p<0.05, **p<0.01, ***p<0.001, and ****p<0.0001.
240
241

Figure 1

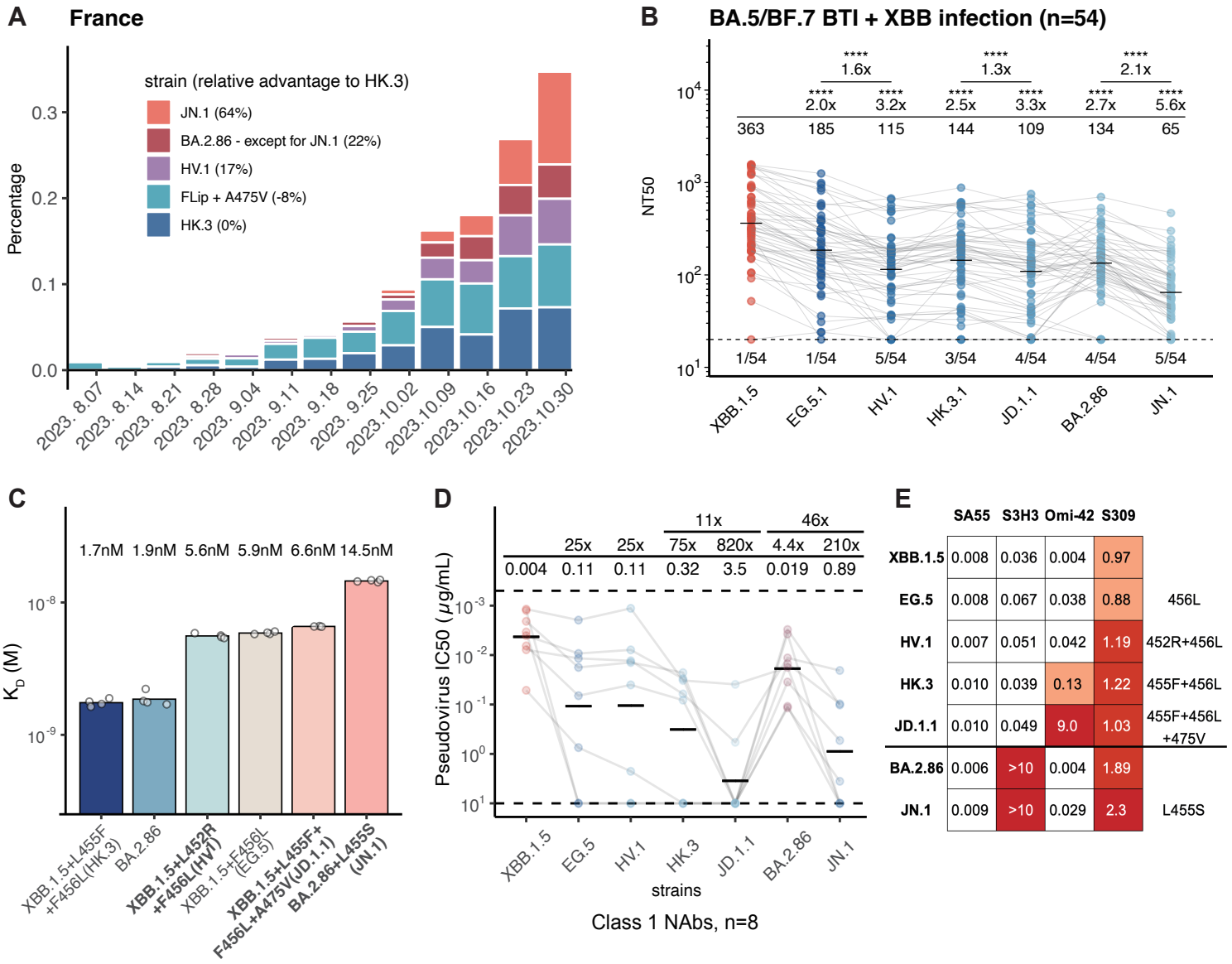
A
France
strain (relative advantage to HK.3)
JN.1 (64%)
BA.2.86 - except for JN.1 (22%)
HV.1 (17%)
FLip + A475V (-8%)
HK.3 (0%)
Percentage
0.0
0.1
0.2
0.3
2023. 8.07
2023. 8.14
2023. 8.21
2023. 8.28
2023. 9.04
2023. 9.11
2023. 9.18
2023. 9.25
2023.10.02
2023.10.09
2023.10.16
2023.10.23
2023.10.30
B
BA.5/BF.7 BTI + XBB infection (n=54)
NT50
1.6x
1.3x
2.1x
2.0x
3.2x
2.5x
3.3x
2.7x
5.6x
363
185
115
144
109
134
65
1/54
1/54
5/54
3/54
4/54
4/54
5/54
XBB.1.5
EG.5.1
HV.1
HK.3.1
JD.1.1
BA.2.86
JN.1
C
1.7nM 1.9nM 5.6nM 5.9nM 6.6nM 14.5nM
K_D (M)
XBB.1.5+L455F +F456L(HK.3)
BA.2.86
XBB.1.5+L452R +F456L(HV1)
XBB.1.5+F456L (EG.5)
XBB.1.5+L455F+ F456L+A475V(JD.1.1)
BA.2.86+L455S (JN.1)
D
11x
46x
25x
25x
75x
820x
4.4x
210x
0.004
0.11
0.11
0.32
3.5
0.019
0.89
Pseudovirus IC50 (μg/mL)
strains
Class 1 NAbs, n=8
E
SA55 S3H3 Omi-42 S309
XBB.1.5 0.008 0.036 0.004 0.97
EG.5 0.008 0.067 0.038 0.88 456L
HV.1 0.007 0.051 0.042 1.19 452R+456L
HK.3 0.010 0.039 0.13 1.22 455F+456L
JD.1.1 0.010 0.049 9.0 1.03 455F+456L +475V
BA.2.86 0.006 >10 0.004 1.89
JN.1 0.009 >10 0.029 2.3 L455S

Figure S1

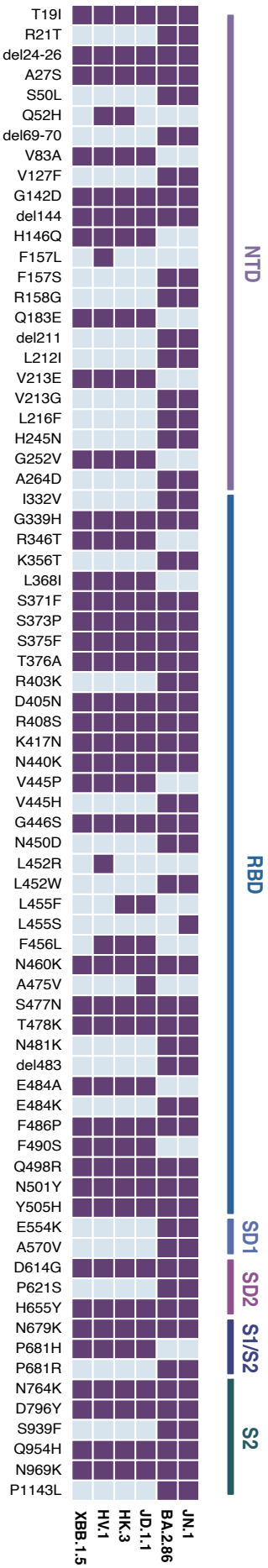
XBB.1.5
HV.1
HK.3
JD.1.1
BA.2.86
JN.1
T19I
R21T
del24-26
A27S
S50L
Q52H
del69-70
V83A
V127F
G142D
del144
H146Q
F157L
F157S
R158G
Q183E
del211
L212I
V213E
V213G
L216F
H245N
G252V
A264D
I332V
G339H
R346T
K356T
L368I
S371F
S373P
S375F
T376A
R403K
D405N
R408S
K417N
N440K
V445P
V445H
G446S
N450D
L452R
L452W
L455F
L455S
F456L
N460K
A475V
S477N
T478K
N481K
del483
E484A
E484K
F486P
F490S
Q498R
N501Y
Y505H
E554K
A570V
D614G
P621S
H655Y
N679K
P681H
P681R
N764K
D796Y
S939F
Q954H
N969K
P1143L
NTD
RBD
SD1
SD2
S1/S2
S2

Figure S2

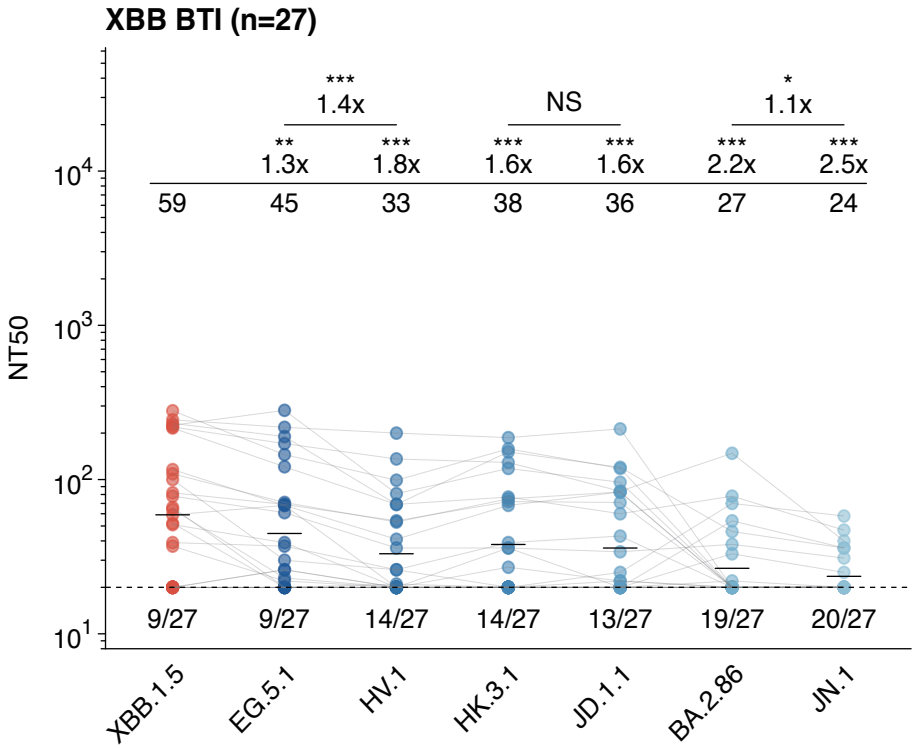
XBB BTI (n=27)
NT50
10^4
10^3
10^2
10^1
***
1.4x
NS
*
1.1x
**
1.3x
***
1.8x
***
1.6x
***
1.6x
***
2.2x
***
2.5x
59
45
33
38
36
27
24
9/27
9/27
14/27
14/27
13/27
19/27
20/27
XBB.1.5
EG.5.1
HV.1
HK.3.1
JD.1.1
BA.2.86
JN.1